Appl. Phys. B 88, 141–150 (2007)
DOI: 10.1007/s00340-007-2647-1

Applied Physics B
Lasers and Optics

N. CHAI[1]
W.D. KULATILAKA[1]
S.V. NAIK[1,✉]
N.M. LAURENDEAU[1]
R.P. LUCHT[1]
J.P. KUEHNER[2]
S. ROY[3]
V.R. KATTA[3]
J.R. GORD[4]

Nitric oxide concentration measurements in atmospheric pressure flames using electronic-resonance-enhanced coherent anti-Stokes Raman scattering

[1] School of Mechanical Engineering, Purdue University, West Lafayette, IN 47907, USA
[2] Department of Physics and Engineering, Washington & Lee University, Lexington, VA 24450, USA
[3] Innovative Scientific Solutions, Inc., 2766 Indian Ripple Road, Dayton, OH 45440, USA
[4] Air Force Research Laboratory, Propulsion Directorate, Wright-Patterson AFB, OH 45433, USA

Received: 12 December 2006/
Revised version: 28 February 2007
Published online: 17 May 2007 •

ABSTRACT We report the application of electronic-resonance-enhanced coherent anti-Stokes Raman scattering (ERE-CARS) for measurements of nitric oxide concentration ([NO]) in three different atmospheric pressure flames. Visible pump (532 nm) and Stokes (591 nm) beams are used to probe the Q-branch of the Raman transition. A significant resonance enhancement is obtained by tuning an ultraviolet probe beam (236 nm) into resonance with specific rotational transitions in the ($v' = 0$, $v'' = 1$) vibrational band of the $A^2\Sigma^+$–$X^2\Pi$ electronic system of NO. ERE-CARS spectra are recorded at various heights within a hydrogen-air flame producing relatively low concentrations of NO over a Hencken burner. Good agreement is obtained between NO ERE-CARS measurements and the results of flame computations using UNICORN, a two-dimensional flame code. Excellent agreement between measured and calculated NO spectra is also obtained when using a modified version of the Sandia CARSFT code for heavily sooting acetylene-air flames ($\phi = 0.8$ to $\phi = 1.6$) on the same Hencken burner. Finally, NO concentration profiles are measured using ERE-CARS in a laminar, counter-flow, non-premixed hydrogen-air flame. Spectral scans are recorded by probing the Q_1 (9.5), Q_1 (13.5) and Q_1 (17.5) Raman transitions. The measured shape of the [NO] profile is in good agreement with that predicted using the OPPDIF code, even without correcting for collisional effects. These comparisons between [NO] measurements and predictions establish the utility of ERE-CARS for detection of NO in flames with large temperature and concentration gradients as well as in sooting environments.

PACS 07.88.+y; 42.62.Fi; 42.65.Dr

1 Introduction

Emissions of oxides of nitrogen (NO_x) from internal combustion and gas turbine engines is a major environmental concern, owing to the direct impact of nitrogenous species on the formation of photochemical smog and their role in global warming via depletion of the ozone layer. Combustion processes contribute about 95% of atmospheric NO_x and a majority of the NO_x from combustion sources is emitted in the form of nitric oxide (NO). Consequently, development of combustors producing low NO levels is an important task facing the combustion community; moreover, such combustors benefit from advances in fundamental knowledge regarding formation and destruction of NO in flame environments.

Laser-induced fluorescence (LIF) is frequently used for the measurement of minor species concentrations in flames, owing to its sensitivity, excellent spatial resolution and experimental simplicity. Many researchers have developed LIF strategies for quantitative detection of nitric oxide in high-pressure flames [1–5]. However, fluorescence signals from NO can become difficult to interpret, especially with increasing pressure, owing to: (a) interferences from oxygen in fuel-lean regions and from hydrocarbons or soot in fuel-rich regions, (b) quenching of the LIF signal via collisions with O_2, CO_2 and H_2O, among other colliding partners, and (c) absorption of both the laser beam and the fluorescence signal by CO_2, H_2O or hydrocarbons at typical UV excitation wavelengths.

Recently, quantification of NO LIF in a heavy-duty Diesel engine was demonstrated by correcting for attenuation of the laser beam and of the NO fluorescence signal arising from CO_2 and O_2 absorption [6, 7]. Additional corrections were made for nitrogen Raman scattering and for window fouling arising from soot. A combination of one-dimensional spectral line-imaging and spatially-resolved, two-dimensional NO-LIF in conjunction with a new multi-spectral detection strategy has also been utilized to quantify measurements in laminar, premixed methane-air flames at pressures up to 60 bar [8]. In addition, a two-photon LIF technique has been developed and applied to study in-cylinder Diesel combustion, eliminating many difficulties associated with the more common single-photon NO LIF [9].

While laser-induced fluorescence techniques are attractive, due to their simplicity and the substantial progress being made to overcome challenges in quantification of NO via LIF, other researchers have considered diagnostic techniques such as cavity ring-down spectroscopy, laser-induced polar-

✉ Fax: +1-765-494-0539, E-mail: naiks@ecn.purdue.edu

ization spectroscopy, and coherent anti-Stokes Raman scattering. While most practical combustion devices operate at high pressure, the robustness and utility of such alternative techniques must first be tested in atmospheric pressure flames.

Conventional coherent anti-Stokes Raman scattering (CARS) has previously been applied to NO measurements in the temperature range from 300 to 800 K at atmospheric pressure [10]. The detection limit for NO was found to be about 2500 ppm in N_2 buffer gas. In a subsequent effort, CARS was utilized to measure the reduction in NO resulting from a microwave generated nitrogen plasma at atmospheric pressure [11]. A polarization sensitive background suppression scheme was applied to detect NO concentrations down to a few hundred ppm.

A significant enhancement in the CARS detection limit can be obtained by tuning one or more of the pump, Stokes and probe beams into resonance with a suitable electronic transition. Previously, such electronic-resonance-enhanced (ERE) CARS has been applied successfully to selected radical species. For example, hydroxyl (OH) concentrations were measured in a low-pressure microwave discharge as well as in atmospheric-pressure, premixed hydrogen-air and methane-air flames [12]. ERE-CARS detection of OH was also demonstrated in laminar, flat flames at pressures up to 9.6 bar [13]. In a later investigation, methylidyne (CH) concentrations were measured in a low-pressure $H_2/CH_4/Ar$ microwave plasma using both LIF and ERE-CARS [14].

For these previous explorations of resonance-enhanced CARS [12–14], the pump, Stokes and probe beams were all at ultraviolet frequencies. In contrast, an ERE-CARS technique has recently been reported which implements an ultraviolet probe beam in electronic resonance while using visible pump and Stokes beams far from electronic resonance [15–18]. By employing a room-temperature jet of 1000 ppm NO in N_2, with substitution of N_2 buffer gas by up to 82% O_2 or CO_2, the NO ERE-CARS signal was shown to display little sensitivity to electronic quenching [16]. This finding is important for many practical combustors, for which the quenching environment can undergo rapid spatial and temporal variations. The pressure dependence of the ERE-CARS signal from 300 ppm NO in N_2 has also been studied within a gas cell at pressures up to 8 bar [17]. The NO ERE-CARS signal increased from 0.1 to 2 bar and remained approximately constant at pressures up to 8 bar. Finally, ERE-CARS has recently been applied to an atmospheric pressure hydrogen-air flame stabilized on a Hencken burner. By doping known quantities of NO into the flame, a detection limit of approximately 50 ppm was demonstrated [18].

In this paper, we present NO measurements via ERE-CARS for three different flame environments, as shown in Fig. 1. Our goal was to assess further the applicability of ERE-CARS for detection of NO in flames with low NO concentrations, with sooting interferences, and with steep temperature and concentration gradients. First, a hydrogen-air flame was stabilized using a Hencken burner and ERE-CARS measurements of NO were obtained at various heights above the burner surface. The measured NO profile was compared with calculations using a detailed reactive flow code. In a second set of experiments, heavily sooting acetylene-air flames were stabilized using the same Hencken burner and spectral scans

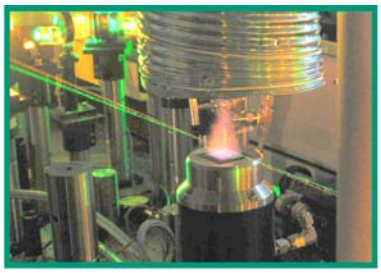

a Non-sooting hydrogen-air ($\phi = 1.15$) flame on a Hencken burner

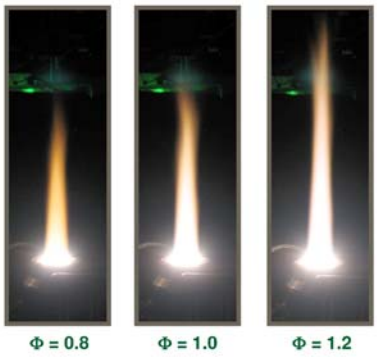

b Sooting C_2H_2-air flames on a Hencken burner

c Non-premixed hydrogen-air flame within a counter-flow burner

FIGURE 1 Three different types of flames investigated in this study

were recorded at various equivalence ratios to demonstrate detection of NO, despite interferences typically precluding LIF measurements. A third set of measurements was performed in a counter-flow flame. The counter-flow configuration produces flat flames having a one-dimensional structure, which permits direct modeling of interactions between fluid mixing and chemical kinetics, thus promoting reliable calculations of flame structure and pollutant formation. Before applying ERE-CARS to NO measurements in high-pressure gas turbine combustors, we must unravel several diagnostic issues in atmospheric pressure, laboratory-scale counter-flow flames, which provide not only a challenging measurement environment but also a good diagnostic test from the perspective of chemical kinetics. Therefore, a laminar, non-premixed, hydrogen-air flame at a global strain rate of 20 s^{-1} was stabilized using a counter-flow burner. In particular, this flame exhibits steep spatial gradients in both temperature and species concentrations. NO concentration profiles were measured in this flame using three different Raman transitions. Measured NO profiles were then compared with concentration profiles computed using an opposed-flow flame code.

2 Experiment

A two-dimensional, non-premixed, near-adiabatic Hencken burner (Research Technologies Model RD15X15) was used to stabilize the atmospheric-pressure hydrogen-air and acetylene-air flames. An oxidizer mixture of 79% N_2 and 21% O_2 was employed instead of commercial air. Mass flow controllers (Models MKS 1559A and M100B) were used to regulate gas flow into the burner. The burner surface is fabricated from a 36.5-mm square hastalloy honeycomb through which the oxidizer flows. The honeycomb structure supports stainless steel fuel tubes in every fourth honeycomb cell. Fuel and oxidizer remain separated before exiting at the burner surface. The burner is designed so as to ensure rapid mixing of fuel and oxidizer immediately above the burner. A co-flow of nitrogen gas was used in the region surrounding the 36.5-mm square honeycomb to shroud the flame. A more detailed description of the Hencken burner is given elsewhere [19]. The burner is mounted on a translation stage that permits horizontal and lateral positioning so as to adjust the ERE-CARS probe volume within the flame. A linear dial gauge was used to measure vertical movement of the burner so that spectra could be recorded at known heights above the burner surface.

The counter-flow burner consists of two 1.9-cm diameter nozzles made of hastalloy C-276 designed to carry either the fuel or oxidizer mixture. The nozzles are water-cooled to prevent overheating and the water temperature is maintained around 30 °C so as to avoid condensation on nozzle surfaces. An annular region surrounding the main reactant tube provides a nitrogen shroud which surrounds the nearly one-dimensional, non-premixed flame stabilized between the opposed nozzles. The separation distance between the fuel and oxidizer nozzles was fixed at 2 cm and the velocity of the reactants at the nozzle exits was maintained at 20 cm/s, thus producing a global strain rate of 20 s^{-1}, where the global strain rate is defined as the sum of reactant velocities at the nozzle exits divided by the nozzle separation distance. The counter-flow burner facility is described in more detail in a previous publication [20].

An energy-level diagram describing the ERE-CARS process for nitric oxide is shown in Fig. 2. The pump (ω_1) and Stokes (ω_2) lasers are visible beams with frequencies far detuned from the $A^2\Sigma^+$–$X^2\Pi$ electronic system of the NO molecule. In contrast, the probe beam frequency (ω_3) is at or near electronic resonance. The CARS signal (ω_4) is generated using a three-dimensional phase-matching geometry. Figure 3 shows a schematic diagram of the experimental system. The second harmonic output (~ 532 nm) of an injection-seeded, Q-switched Nd:YAG laser was used as the pump beam. This second harmonic output was also used to pump a narrow-band dye laser to produce tunable radiation in the vicinity of 704 nm. The output of the dye laser was frequency-mixed with the third harmonic output (~ 355 nm) of the injection-seeded YAG laser to generate the probe beam (~ 236 nm). The second harmonic output of a separate unseeded, Q-switched Nd:YAG laser was used to pump another narrow-band dye laser to produce tunable radiation in the vicinity of 591 nm, which acts as the Stokes beam. The full-width at half-maximum (FWHM) linewidth of the pump beam

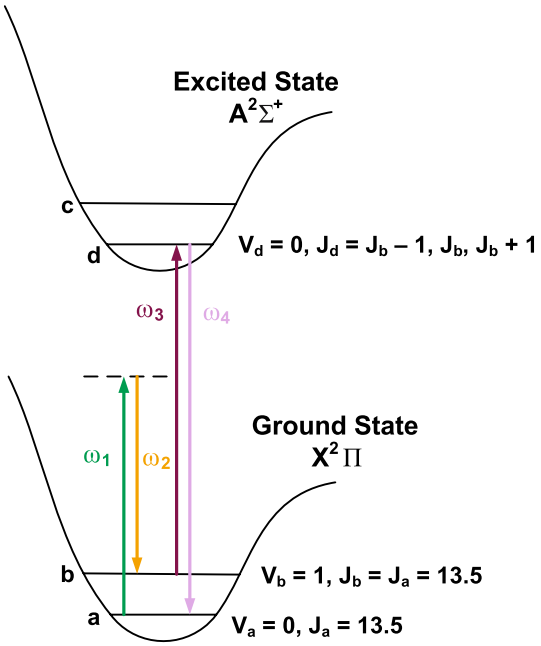

FIGURE 2 Energy level diagram showing the ERE-CARS process for NO. The transitions identify the pump beam ($\omega_1 = 18\,789.4\ cm^{-1}$), Stokes beam ($\omega_2 = 16\,920.5\ cm^{-1}$), probe beam ($\omega_3 = 42\,372.8\ cm^{-1}$) and CARS signal beam ($\omega_4 = 44\,241.7\ cm^{-1}$)

(532 nm) was 0.003 cm^{-1} while the linewidths for the Stokes (591 nm) and the probe (236 nm) beams were 0.1 cm^{-1}. Using a translating razor blade, we measured the diameters of the three beams 20 mm away from the focus (CARS probe volume) to be approximately 250 μm.

A polarization-sensitive technique was employed to suppress the non-resonant background signal arising from four-wave mixing. The probe beam was vertically polarized while the polarizations of the pump and Stokes beams were set at an angle of 60° with respect to the vertical axis. Fine adjustment of the polarizer in the detection channel, orthogonal to the four-wave mixing signal, enables optimum suppression of any non-resonant background [14].

For experiments performed using the Hencken burner, the ultraviolet probe wavelength was held fixed at 236.06 nm corresponding to the Q_1 (13.5) transition in the (0,1) band of the $A^2\Sigma^+$–$X^2\Pi$ electronic system of NO. Spectra were recorded at various heights above the burner by tuning the wavelength of the visible Stokes beam, so that UV fluorescence interferences and/or background scattering remained constant during the spectral scan. Such scans, for which the Stokes wavelength was varied while the UV probe wavelength was fixed, are referred to as Stokes scans. The resulting baseline can be subtracted to obtain a background-corrected ERE-CARS signal. This background-corrected signal is then divided by the measured UV pulse energy to account for shot-to-shot variations in the energy of the pulsed probe beam.

Three different Raman transitions were investigated for experiments performed using the counter-flow burner. A substantial temperature gradient exists between the fuel and oxidizer streams in the counter-flow configuration. In fact, NO is formed and destroyed over temperatures ranging from 700 K to 2500 K. For these experiments, the Q_1 (9.5), Q_1 (13.5) and Q_1 (17.5) Raman transitions were selected to assess the tem-

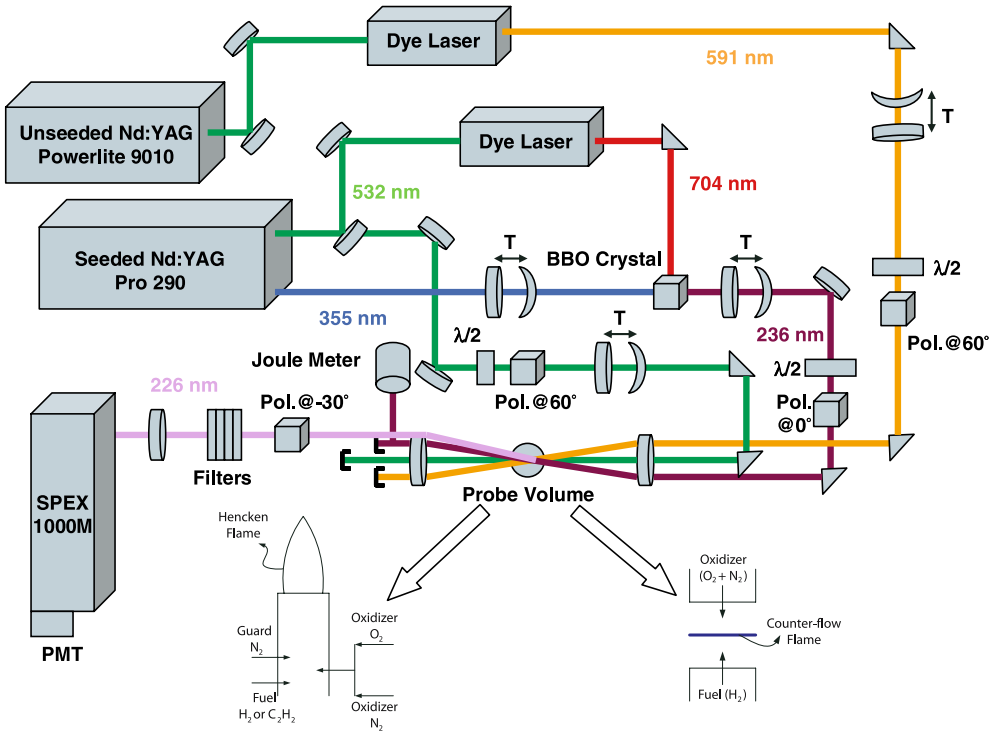

FIGURE 3 Schematic of the experimental setup for ERE-CARS of NO. T: telescope; λ/2: half-wave plate; PMT: photomultiplier tube. Polarizer angles are set with respect to the vertical axis. Filters are composed of four 45°, 215-nm mirrors having 70% transmission at 226 nm and 1% transmission at 236 nm

perature sensitivity of the measured [NO] profile. For the three selected Raman transitions, the ultraviolet probe wavelength was held fixed at 236.19 nm, 236.06 nm and 235.87 nm, respectively, corresponding to the Q_1 (9.5), Q_1 (13.5) and Q_1 (17.5) transitions in the (1,0) band of the $A^2\Sigma^+$–$X^2\Pi$ electronic system of NO. Stokes scans were recorded every one mm between the fuel and oxidizer nozzles for each of the three ERE-CARS transitions.

3 Modeling

Numerical computations for the hydrogen-air flame stabilized using the Hencken burner was performed using the UNICORN (UNsteady Ignition and COmbustion with ReactioNs) code [21–23]. The flame is modeled as a combination of several diffusion flamelets, where each flamelet is supported by fuel originating from each individual tube within the burner. The exact nature of the flamelet (premixed, partially premixed or non-premixed) can be varied, depending on experimental flow conditions. The flamelet established over the fuel tube is modeled as an axi-symmetric flow while the hexagonal opening around the fuel tube, through which the oxidizer mixture flows, is modeled as a co-annular tube. Adiabatic flow conditions are assumed at the fuel-tube wall. Symmetric boundary conditions are employed along the centerline of the flow as well as at the outer boundary in the radial direction of the burner; linear extrapolation of flow variables is implemented along the outflow boundary located at a height of several fuel-tube diameters above the burner surface. Fuel and air velocities are determined from the known mass flow rates of gases.

For the counter-flow flame, OPPDIF, a Sandia opposed-flow flame code [24], was used for calculations of temperature, velocity and species concentration profiles along the centerline between the two nozzles. The mathematical model for OPPDIF reduces the two-dimensional, axi-symmetric flow field to a one-dimensional formulation via a similarity transformation [25]. The GRI mechanism (version 3.0) [26] was used for the chemical kinetics; gas-phase radiation was considered by adding a radiation source term in OPPDIF. The effect of radiative heat loss was considered in the optically thin limit [27]. The radiation model utilizes Planck mean absorption coefficients for the major species CO_2, H_2O, CO and CH_4; the temperature dependence of these coefficients was modeled using fourth-order polynomial fits to the results of narrow-band calculations. A time-dependent, axi-symmetric model in UNICORN was also employed for simulation of a weakly-stretched counter-flow diffusion flame. The two-dimensional calculations were performed on a grid having 801 by 41 nodal points in the axial and radial directions, respectively.

The ERE-CARS spectra were modeled using a perturbative analysis applicable at lower laser irradiances via modification of the Sandia CARSFT code [15, 28]. Spectral data for the NO molecule were obtained via LIFBASE [29] and from high-resolution CARS measurements [30, 31].

4 Results and discussion

Figure 4 displays spectra recorded for various heights in a hydrogen-air flame stabilized on the Hencken burner at $\phi = 1.15$. We previously added known quantities of NO to the oxidizer flow in a similar flame to determine the NO detection limit at atmospheric pressure [18]. From Fig. 4, we find that the NO ERE-CARS signal along the centerline of the flame rises with height above the burner surface. The spectra in Fig. 4 exhibit a non-resonant background resulting from scattering of the UV probe beam and fluorescence induced

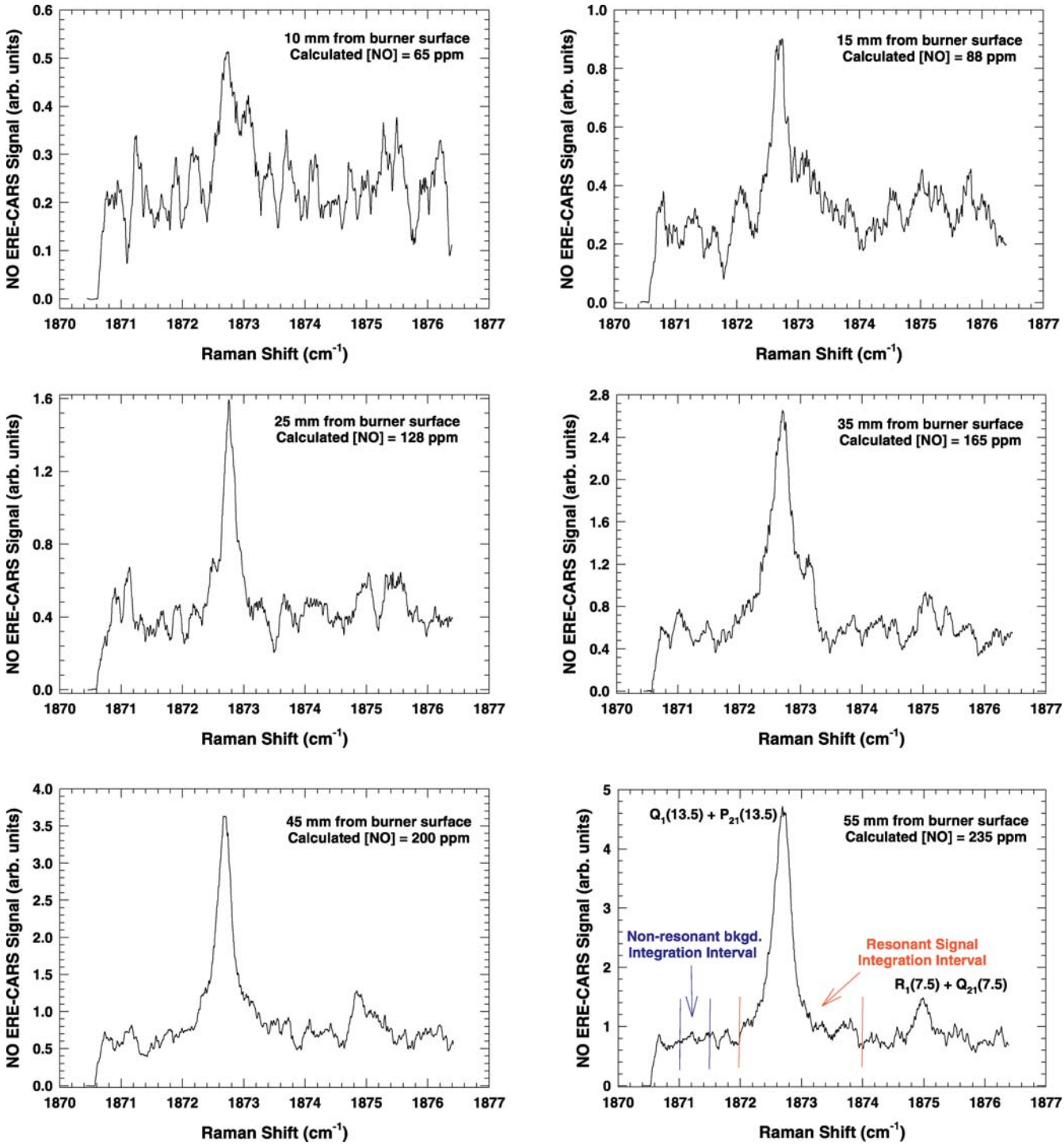

FIGURE 4 Spectral scans at various heights above the Hencken burner in an H_2-air ($\phi = 1.15$) flame. The UV probe frequency was fixed at 42 361.46 cm^{-1}, corresponding to the Q_1 (13.5) transition in the $A^2\Sigma^+ – X^2\Pi$ (1,0) band. Pump, Stokes and probe energy levels were fixed at 14 mJ/pulse, 18 mJ/pulse and 0.6 mJ/pulse, respectively

by the same UV beam. Because the UV probe wavelength is fixed during Stokes scans, this non-resonant background is nominally constant, independent of Stokes laser wavelength. Furthermore, the non-resonant background does not modulate the ERE-CARS signal, so that it can be subtracted in data processing. The overall non-resonant background signal was obtained via integration between Raman shifts of 1871.0 and 1871.5 cm^{-1}. After background subtraction and division by the UV probe energy, the ERE-CARS signal was integrated between Raman shifts of 1872 and 1874 cm^{-1}.

Figure 5 shows a comparison between the measured concentration of NO, which is proportional to the square-root of the integrated ERE-CARS signal, and predicted NO concentrations computed using UNICORN at various heights above the burner surface. As fuel and oxidizer are rapidly mixed in the region above the burner surface, a sharp increase in tem-

perature occurs owing to combustion reactions. In the post-flame regime, the temperature remains essentially constant; however, the NO concentration increases continuously because of the Zeldovich reactions. We should note that the data points are not corrected for variations in Boltzmann fraction, owing to the nearly constant post-flame temperature, as shown in Fig. 5.

Flames encountered in practical applications, such as gas turbine combustors, furnaces and internal combustion engines, are highly luminous and particle laden, especially when using liquid fuels. Hydrocarbon species, their fragments and soot particulates possess very broad absorption and emission signatures throughout the ultraviolet region [32]. Such broadband UV interferences complicate signal interpretation when detecting NO via LIF for excitation near 226 nm in the γ (0,0) band [1–5]. Therefore, acetylene-air flames were studied from lean ($\phi = 0.8$) to rich ($\phi = 1.6$) conditions to assess the feasibility of ERE-CARS measurements under highly sooting conditions. Spectra recorded 55 mm above the burner surface are shown in Fig. 6 along with theoretical spectral fits obtained using the modified Sandia CARSFT code. Good agreement is observed between theory and experiment for these conditions. The excellent selectivity of the ERE-CARS technique arises from the fact that both Raman and electronic resonance conditions must be satisfied to generate the ERE-CARS signal. Based on Fig. 6, ERE-CARS can be employed for detection of NO, even in heavily

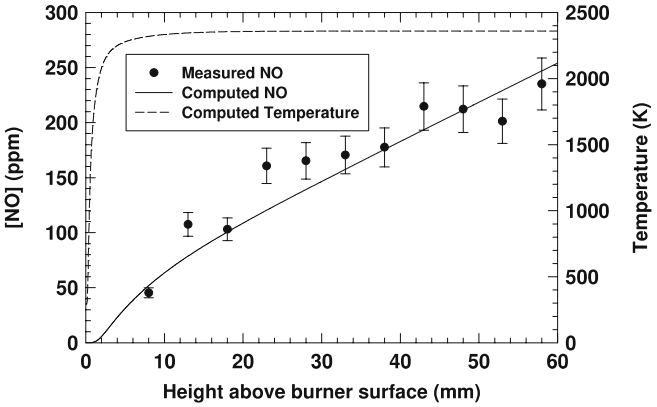

FIGURE 5 Comparison between measured and computed NO concentrations (using UNICORN) at various heights above the Hencken burner in an H_2-air ($\phi = 1.15$) flame. The data were scaled so as to match measured and calculated [NO] at 48 mm above the burner surface. The temperature profile was also calculated using UNICORN

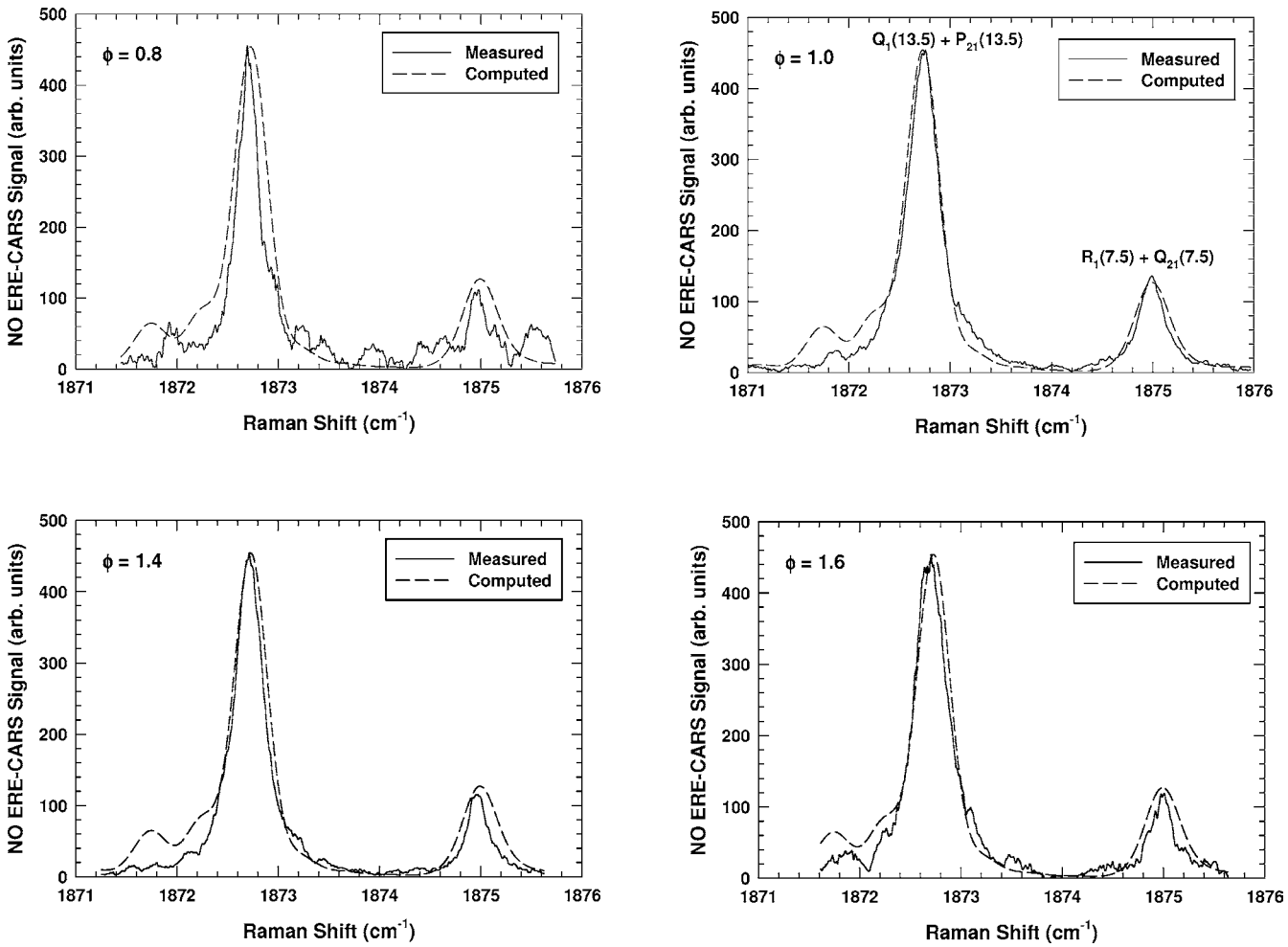

FIGURE 6 Comparisons between measured and computed ERE-CARS spectra at 55 mm above the Hencken burner for highly sooting C_2H_2-air flames. The UV probe frequency was fixed at 42 361.46 cm^{-1}, corresponding to the Q_1 (13.5) transition in the $A^2\Sigma^+$–$X^2\Pi$ (1,0) band. Pump, Stokes and probe energy levels were fixed at 10 mJ/pulse, 16 mJ/pulse and 1.2 mJ/pulse, respectively. For the theoretical calculations, linewidths of the Stokes and probe laser were selected to be 0.37 cm^{-1} and 3 cm^{-1}, respectively. The theoretical fits were obtained using a temperature of 2300 K and an NO concentration of 1000 ppm

sooting flames, thus overcoming one of the major drawbacks of LIF.

Figure 7 displays Stokes spectra recorded at various positions between the fuel and oxidizer nozzle for the non-premixed, hydrogen-air counter-flow flame at a global strain rate of 20 s^{-1}. A significant modulation in ERE-CARS signal is obtained between the fuel and oxidizer nozzles, as shown in Fig. 7. The background-corrected and normalized ERE-CARS signals from these spectra were integrated between Raman shifts of 1871.2 and 1873.8 cm^{-1}. Knowing the computed temperature at each position from OPPDIF, we calculated the Boltzmann fraction for the $J'' = 13.5$, $N'' = 13$, $v'' = 0$ rotational-vibrational level. The square-root of the integrated ERE-CARS signal was then corrected for population

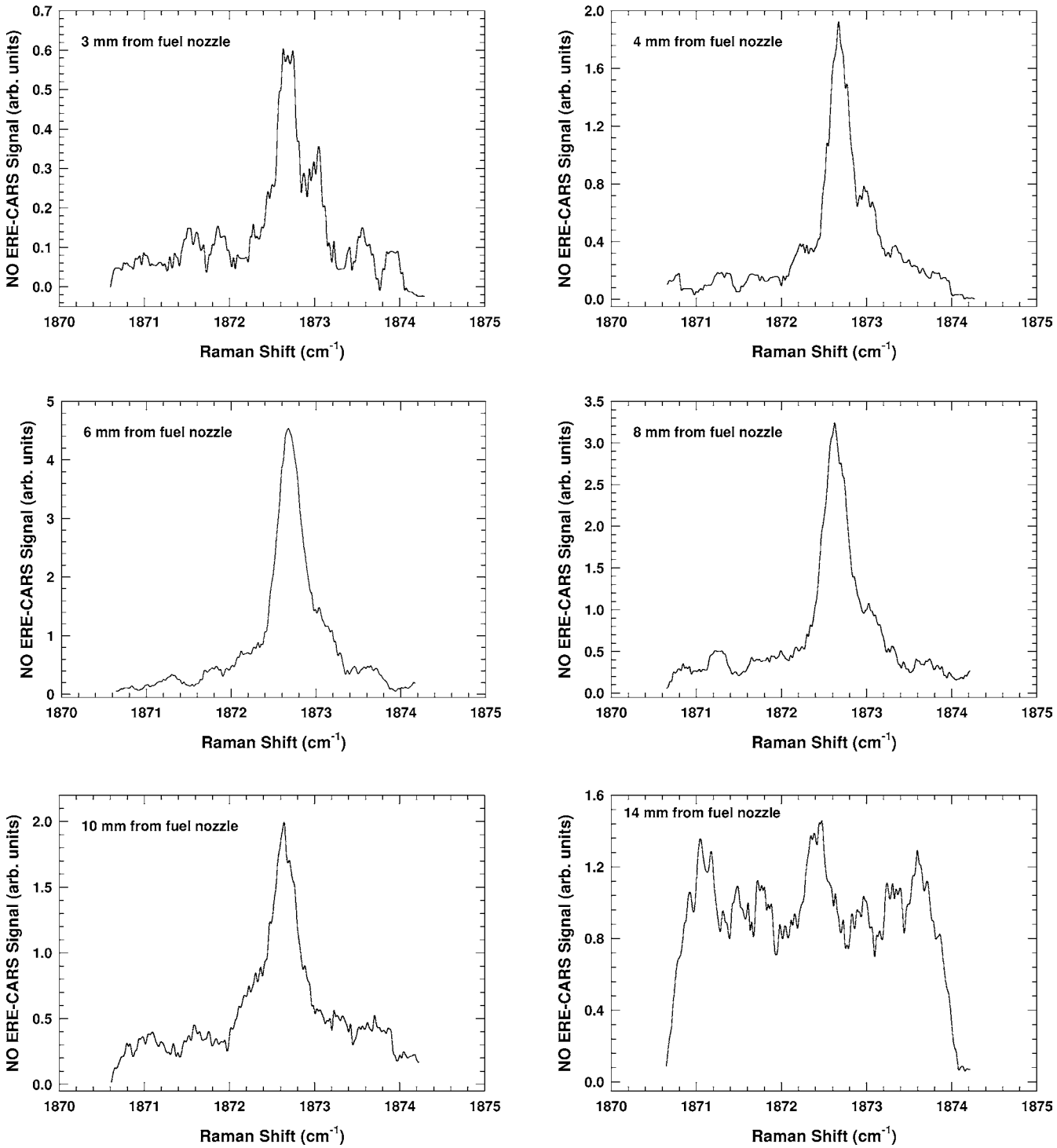

FIGURE 7 Spectral scans indicating NO ERE-CARS signals at various positions in an atmospheric pressure, laminar, counter-flow, non-premixed H_2-air flame at a global strain rate of 20 s^{-1}. The UV probe frequency was fixed at 42 361.46 cm^{-1}, corresponding to the Q_1 (13.5) transition in the $A^2\Sigma^+ – X^2\Pi$ (1,0) band. Pump, Stokes and probe energy levels were fixed at 14 mJ/pulse, 10 mJ/pulse and 0.5 mJ/pulse, respectively

differences using an appropriate calculation of Boltzmann fraction. The integration intervals for the two other Raman transitions, Q_1 (9.5) and Q_1 (17.5), were selected to be 1873 to 1875 cm^{-1} and 1869 to 1872 cm^{-1}, respectively. In Fig. 8, the square-root of the integrated signal, as divided by the Boltzmann fraction for the corresponding rotational level at the calculated temperature, is plotted versus distance between the two nozzles for three different Raman transitions.

The three different profiles were scaled by setting the peak of the Q_1 (13.5) profile to unity. While the profile peaks for the Q_1 (9.5) and Q_1 (17.5) ERE-CARS signals were not scaled to match the Q_1 (13.5) case, the peaks for all three profiles agree to within 15%. This agreement was observed even though measurements for the three different transitions were acquired over several hours, thus indicating the stability of the optical alignment. We observe that the shapes of the NO concentration profiles measured using three different Raman transitions are very similar, and that the peaks of the profiles, corrected for their respective Boltzmann fractions, are in excellent agreement. We should note, however, that in regions of low NO concentration, the integrated ERE-CARS signal is sensitive to any background correction.

The relative agreement, both in terms of spatial location and magnitude, between the experimental and computed [NO] profiles, either using OPPDIF (one-dimensional calculation) or UNICORN (two-dimensional calculation), is quite satisfactory. Indeed, considering potentially complicating factors such as variations in temperature, collisional width and quenching environment in the counter-flow configuration, the excellent agreement between measured and calculated profiles is surely remarkable. Hence, we conclude that the proposed ERE-CARS technique should be applicable in complex collisional environments, while still giving a spatial resolution comparable to techniques such as LIF and CARS.

Figure 9 shows a comparison between measured and predicted NO concentrations, including the variation in calculated temperature, for the counter-flow hydrogen-air flame. Scaling the measured ERE-CARS signals via the predicted peak NO concentration, we estimate a detection limit of ~ 25 ppm for the counter-flow flame measurements using three different Raman transitions. This detection limit could potentially be improved by focusing the beams more tightly and by employing strategies to reduce the UV scattering/fluorescence.

Collisions of the NO molecule with other atoms (e.g., O, H), diatomic radicals (e.g., OH, NO) and major species (e.g., H_2, O_2, H_2O, CO, CO_2, CH_4, N_2) depend on pressure and temperature. It is well-known that LIF signals decrease owing to such collisions, thus requiring corrections for quantification of NO LIF signals. We have previously shown that the ERE-CARS signal is nearly independent of electronic quenching when considering two important colliders, O_2 and CO_2 [16]. In a counter-flow non-premixed flame, temperature and species concentrations vary significantly in the flow field between the fuel and oxidizer nozzles. Figure 10 shows the computed variation in total quenching rate (Fig. 10a) as well as that for the collisional and Doppler linewidths (Fig. 10b) for a non-premixed H_2-air flame. Quenching rate coefficients (cm^3s^{-1}) for collisions of NO with H, H_2, O, O_2, OH, H_2O, N_2, NH, NO, NO_2 and N_2O were obtained from the literature [33]. The number density of each collider and the temperature at different locations were obtained from OPPDIF, with the total quenching rate (s^{-1}) calculated from the sum of individual quenching rates.

As shown in Fig. 10a, the total electronic quenching rate varies considerably in the region encompassing measurable NO concentrations. In practical combustion systems, such variations in quenching rate, both in space and time, can cause substantial variations in signal levels when using LIF. The ERE-CARS spectra recorded using Stokes scans at different positions between the fuel and oxidizer nozzles were analyzed, without correction for variations in the collision rate. Hence, the good agreement between measured and calculated [NO] profiles, as shown in Fig. 8, demonstrates the effectiveness of the ERE-CARS technique despite large variations in collisional rate throughout the flame.

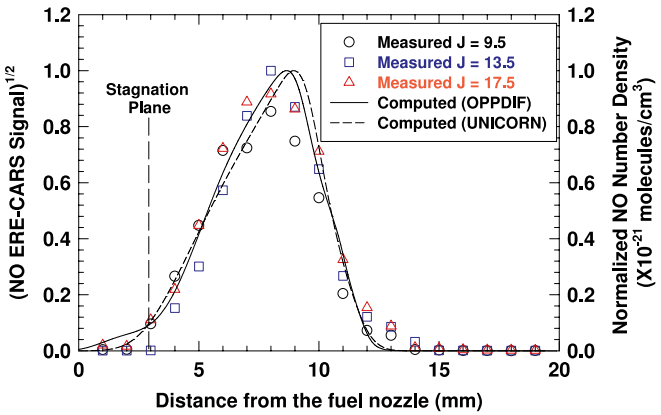

FIGURE 8 Comparison between measured NO signals and computed NO number density in an atmospheric pressure, laminar, counter-flow, non-premixed H_2-air flame at a global strain rate of 20 s^{-1}. The integrated ERE-CARS signal has been corrected through background subtraction, division by the ultraviolet pulse energy, and division by the Boltzmann fraction using temperatures calculated from OPPDIF with GRI 3.0 chemical kinetics. Computed profiles using OPPDIF (one-dimensional calculation) and UNICORN (two-dimensional calculation) match well at the low strain rate of 20 s^{-1}

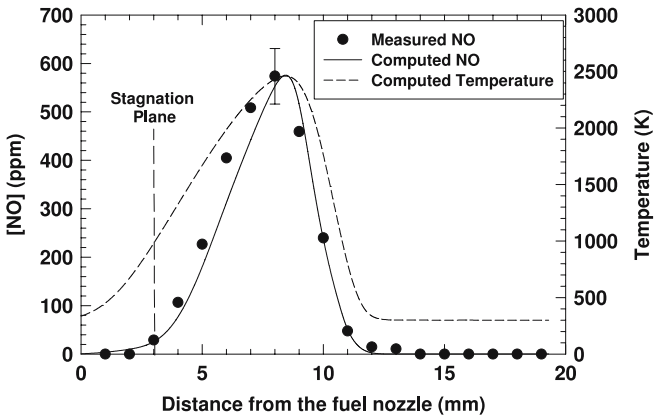

FIGURE 9 Comparison between measured and computed NO concentrations in an atmospheric pressure, laminar, counter-flow, non-premixed H_2-air flame at a global strain rate of 20 s^{-1}. Data points were obtained by averaging the ERE-CARS measurements shown in Fig. 8 at each position, calibrating using the computed maximum NO number density, and converting from number density to ppm levels using temperatures calculated from OPPDIF with GRI 3.0 chemical kinetics

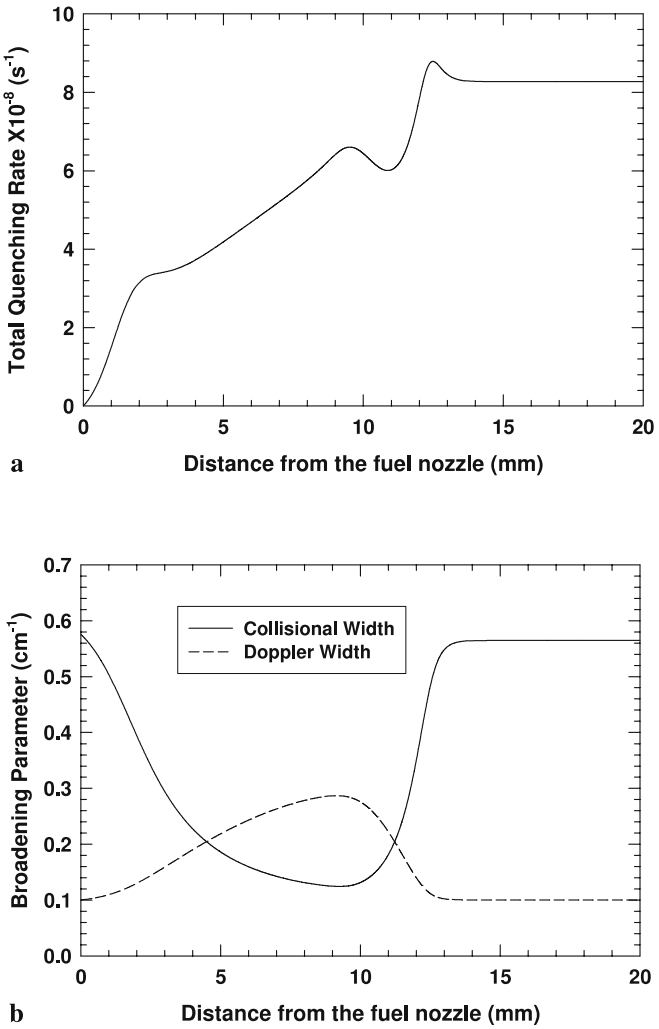

FIGURE 10 Variation of (**a**) total electronic quenching rate and (**b**) collisional and Doppler widths in an atmospheric pressure, laminar, counter-flow, non-premixed H_2-air flame at a global strain rate of 20 s^{-1}. Temperature and species concentrations are obtained from OPPDIF using GRI 3.0 chemical kinetics

The CARS signal generated from the probe volume depends on the square of the third order non-linear susceptibility; the exact scaling is affected by the broadening mechanism for both the Raman transition and the UV probe transition, as well as on the transition spacing. Although much information is available on collisional broadening of ultraviolet transitions, little information is available on NO Raman linewidths at flame conditions. As the temperature increases from about 350 K in the wings of the NO profile to about 2500 K near the [NO] peak, the density decreases which produces a reduction in the collision-broadened linewidth. The Doppler width, on the other hand, increases somewhat in the high-temperature region, although at atmospheric pressure the Raman transition is predominantly collision-broadened even at flame temperatures. Figure 10b shows this variation in computed collisional and Doppler widths between the two nozzles. In the region between 4 to 12 mm from the fuel-side nozzle, the ratio of collisional to Doppler widths changes by over a factor of two. Such variations could cause substantial changes in laser interaction with the Raman and probe transitions, thus potentially complicating the interpretation of ERE-CARS signals. However, based on Fig. 8, for which the experimental concentration profile was corrected only for changes in temperature, the measured NO profile still agrees very well with computations using rigorous transport and chemical kinetics. The factors which lead to such good agreement will be explored in future work. In particular, our intention is to investigate saturation effects on the Raman transition and/or the UV probe transition.

5 Conclusions

ERE-CARS was applied successfully to NO concentration measurements in three different atmospheric pressure flames. Stokes scans were recorded at various heights in a slightly rich ($\phi = 1.15$) hydrogen-air flame stabilized on a Hencken burner. The axial profile of the background-corrected, square-root of the NO ERE-CARS signal proved to be in excellent agreement with calculated NO concentration profiles. Background-corrected detection of NO was also demonstrated in acetylene-air flames under both fuel-lean and highly sooting fuel-rich conditions. Excellent agreement was obtained between measured and theoretical spectra when using a modified Sandia CARSFT code. Finally, an atmospheric-pressure, laminar, counter-flow non-premixed hydrogen-air flame was investigated at a global strain rate of 20 s^{-1}. Despite considerable variation in collisional and Doppler linewidths, the measured and computed NO concentration profiles were found to be in excellent agreement.

The above three experiments demonstrate that ERE-CARS is a robust diagnostic technique which can be used to detect flame-generated NO in challenging environments. The ERE-CARS signal appears to be much less dependent on collisional rates, especially electronic quenching rates, than is the case for NO LIF. Continuing efforts will focus on understanding the physics of the ERE-CARS process, on further development of the technique to enable single-shot measurements, and on applications of ERE-CARS to high-pressure laboratory flames as well as to gas-turbine combustors.

ACKNOWLEDGEMENTS Funding for this research was provided by the U.S. Department of Energy, Division of Chemical Sciences, Geosciences and Biosciences, under Grant No. DE-FG02-03ER15391, by the Air Force Office of Scientific Research under Contract No. FA9550-05-C-0096 (Dr. Julian Tishkoff, Program Manager), and by the Air Force Research Laboratory, Propulsion Directorate, Wright-Patterson Air Force Base, under Contract No. F33615-03-D-2329.

REFERENCES

1 C.S. Cooper, N.M. Laurendeau, Appl. Phys. B **70**, 903 (2000)
2 W.G. Bessler, C. Schulz, T. Lee, J.B. Jeffries, R.K. Hanson, Appl. Opt. **41**, 3547 (2002)
3 W.G. Bessler, C. Schulz, T. Lee, J.B. Jeffries, R.K. Hanson, Appl. Opt. **42**, 2031 (2003)
4 W.G. Bessler, C. Schulz, T. Lee, J.B. Jeffries, R.K. Hanson, Appl. Opt. **42**, 4922 (2003)
5 S.V. Naik, N.M. Laurendeau, Combust. Sci. Technol. **174**, 1809 (2004)
6 K. Verbiezen, R.J.H. Klein-Douwel, A.P. van Vliet, A.J. Donkerbroek, W.L. Meerts, N.J. Dam, J.J. ter Meulen, Appl. Phys. B **83**, 155 (2006)
7 K. Verbiezen, R.J.H. Klein-Douwel, A.P. van Vliet, A.J. Donkerbroek, W.L. Meerts, N.J. Dam, J.J. ter Meulen, Proc. Combust. Inst. **31**, 765 (2007)
8 T. Lee, J.B. Jeffries, R.K. Hanson, Proc. Combust. Inst. **31**, 757 (2007)
9 G.C. Martin, C.J. Mueller, C.F. Lee, Appl. Opt. **45**, 2089 (2006)

10 T. Doerk, J. Ehlbeck, R. Jedamzik, J. Uhlenbusch, J. Hoschele, J. Steinwandel, Appl. Spectrosc. **51**, 1360 (1997)
11 A. Pott, T. Doerk, J. Uhlenbusch, J. Ehlbeck, J. Hoschele, J. Steinwandel, J. Phys. D Appl. Phys. **31**, 2485 (1998)
12 B. Attal-Tretout, P. Berlemont, J.P. Taran, Mol. Phys. **70**, 1 (1990)
13 B. Attal-Tretout, S.C. Schmidt, E. Crete, P. Dumas, J.P. Taran, J. Quantum Spectrosc. Radiat. Transf. **43**, 351 (1990)
14 P. Doerk, M. Hertl, B. Pfelzer, S. Hadrich, P. Jauernik, J. Uhlenbusch, Appl. Phys. B **64**, 111 (1997)
15 S.F. Hanna, W.D. Kulatilaka, Z. Arp, T. Opatrny, M.O. Scully, J.P. Kuehner, R.P. Lucht, Appl. Phys. Lett. **83**, 1887 (2003)
16 S. Roy, W.D. Kulatilaka, S.V. Naik, N.M. Laurendeau, R.P. Lucht, J.R. Gord, Appl. Phys. Lett. **89**, 104 105 (2006)
17 W.D. Kulatilaka, N. Chai, S.V. Naik, N.M. Laurendeau, R.P. Lucht, J.P. Kuehner, S. Roy, J.R. Gord, Opt. Commun. **274**, 441 (2007)
18 W.D. Kulatilaka, N. Chai, S.V. Naik, N.M. Laurendeau, R.P. Lucht, J.P. Kuehner, S. Roy, J.R. Gord, Opt. Lett. **31**, 3357 (2006)
19 W.D. Kulatilaka, R.P. Lucht, S.F. Hanna, V.R. Katta, Combust. Flame **137**, 523 (2004)
20 N. Vora, J.E. Siow, N.M. Laurendeau, Combust. Flame **126**, 1393 (2001)
21 V.R. Katta, L.P. Goss, W.M. Roquemore, Combust. Flame **96**, 60 (1994)
22 V.R. Katta, L.P. Goss, W.M. Roquemore, AIAA J. **32**, 84 (1994)
23 V.R. Katta, L.P. Goss, W.M. Roquemore, Int. J. Numer. Methods Heat Fluids Flow **4**, 413 (1994)
24 A.E. Lutz, R.J. Kee, J.F. Grcar, Sandia National Laboratories, Report No. SAND96-8243 (1996)
25 R.J. Kee, J.A. Miller, G.H. Evans, G. Dixon-Lewis, Proc. Combust. Inst. **22**, 1479 (1988)
26 G.P. Smith, D.M. Golden, M. Frenklach, N.W. Moriarty, B. Eiteneer, M. Goldenberg, C.T. Bowman, R.K. Hanson, S. Song, W.C. Gardiner Jr., V. Lissianski, Z. Qin, GRI Mechanism (version 3.0) http://www.me.berkeley.edu/gri_mech/ (1999)
27 J.P. Gore, J. Lim, T. Takeno, X.L. Zhu, Proceedings of Fifth ASME/JSME Joint Thermal Engineering Conference, San Diego, CA, Paper AJTE99-6311 (1999)
28 R.E. Palmer, Sandia National Laboratories, Report No. SAND89-8206 (1989)
29 J. Luque, D.R. Crosley, SRI International, Report. No. MP99-009 (1999)
30 J. Laane, W. Kiefer, J. Raman Spectrosc. **9**, 353 (1980)
31 W. Lempert, G.J. Rosasco, W.S. Hurst, J. Chem. Phys. **81**, 4241 (1984)
32 A.C. Eckbreth, *Laser Diagnostics for Combustion Temperature and Species* (Gordon and Breach, Amsterdam, 1996)
33 P.H. Paul, C.D. Carter, J.A. Gray, J.W. Thoman, M.R. Furlanetto, Sandia National Laboratories, Report No. SAND94-8237 (1995)